INTERNATIONAL JOURNAL FOR NUMERICAL METHODS IN FLUIDS VOL. 5, 155–167 (1985)

TURBULENT FLOW IN A DUCT WITH CUSPED CORNERS

C. W. RAPLEY

Department of Mechanical Engineering, Sunderland Polytechnic, Sunderland, England

SUMMARY

An orthogonal-cuvilinear-mesh-based finite volume calculation method has been applied to the problem of fully developed turbulent flow in the tri-cusped cornered duct formed when parallel circular rods touch in triangular array. Algebraic stress relations combined with the k–ε turbulence model are used for calculation of the required stresses. A single circulation of turbulence-driven cross-plane secondary flow from the core into the duct corner has been predicted in a one-sixth symmetry region of the duct and the convective transport effects of this flow are seen to have much influence on local mean flow distributions. The turbulence field predicted by the k–ε model showed significant damping in the cusped corner region where turbulent viscosities approached the laminar value. Satisfactory agreement was obtained with the limited local and overall mean flow measurements available.

KEY WORDS Turbulent Flow Tri-cusped Duct Finite Volume

INTRODUCTION

The need for compact flow passages in heat exchangers and other flow systems often leads to the consideration of ducts with small internal angles or with walls that meet tangentially to form cusped corners. Examples can be found in the 'sine-duct' and other passages formed from alternate layers of corrugated and flat material (Figure 1(a)), between rods in rod or tube bundles (Figure 1(b)) and also between the shell and tubes (Figure 1(c)) or in moon-shaped ducts (Figure 1(d)). The rapid change in flow cross-section of these ducts will give rise to relatively large variations in axial velocity across the flow and in wall shear stress and heat flux around the periphery which will feature markedly in design considerations. The restricted access in this type of passage causes obvious measurement difficulties and will account for the paucity of turbulent local mean flow and heat transfer experimental data currently available (see for example Reference 1).

For these reasons the availability of a reliable turbulent flow prediction procedure, to supplement and extend experiment, would be a decided advantage. However, the development of such a method is hampered by the difficult geometry of the ducts and the significant influence of secondary flows which makes the calculation of a three dimensional velocity field usually necessary for fully developed flow. Simplified approaches, allowing indirectly for secondary flow effects, cannot usually simulate the full influences on local mean flow.[2]

The presence of turbulence driven secondary flows in the passage cross-plane of straight non-circular passages has been known since the early experiments of Nikuradse[3] in triangular and other shaped ducts, where the measured axial velocity contours showed distortions that were attributed to secondary flows. These distortions were a general bulging of axial velocity contours

0271–2091/85/02 0155–13$01.30

Received 2 December 1983
Revised 6 April 1984

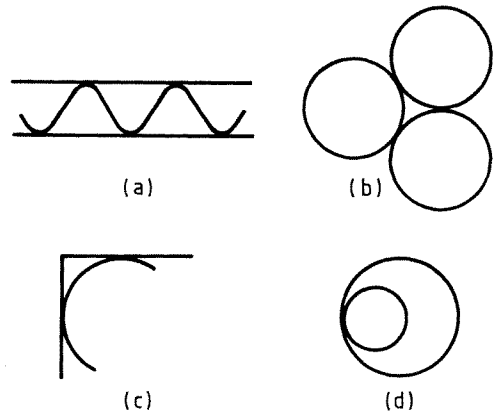

Figure 1. Examples of ducts with cusped corners

into duct corners, a feature which has now become a characteristic effect of secondary motions on the mean flow in non-circular passages. Since Nikuradse's work actual measurements of secondary velocities, usually found to be of the order of 1–2 per cent of mean axial velocity, have been reported for square and rectangular ducts,[4–6] an equilateral triangular duct[7] and a rod bundle passage.[8] The general pattern of secondary flow circulation found was from the core into duct corners along the region around the corner bisectors, returning to the core via the wall region and planes normal to the wall. This convective transport of higher velocity core fluid towards the duct corners accounts for the observed bulging of axial velocity contours in that direction. Indeed, turbulent flow calculations which included secondary flow in these passages,[7,9,10] indicate that the secondary motions have a marked effect generally on local mean flow distributions.

The above calculations have been mainly test cases presented as part of the validation procedures for the methods developed and thus have relatively uncomplicated non-circular passage geometries. This is confirmed by the overall axial pressure-drop or friction factors which were generally similar to circular pipe values when the equivalent (hydraulic) diameter was used. There do not appear to be any comparable theoretical studies of ducts which are very non-circular, such as those with cusped or very narrow internal corners, and this situation has been the main spur to the present work.

The duct shown in Figure 1(b) is of particular interest because it represents the limiting case of compact rod bundle flows with rods touching in triangular array. Closely spaced rod bundles have important applications in nuclear reactor cores and other compact heat exchangers and, over the years, much effort has gone into methods of prediction.[11–16] However, no calculations of turbulent flow with predicted secondary flow appear to be available for rods closer than a pitch (P)/diameter (D) ratio of 1·1.[10,17,18] The duct in Figure 1(b) yields a very non-circular passage shape with curved walls and cusped corners and is thus suitable for the present study. This should provide useful information on local mean flow, secondary flow and turbulence distributions and the problems associated with their prediction generally in this class of duct as well as specifically for the limiting case of rods touching in rod bundle flow.

Experimental work on turbulent flow in this duct geometry is mainly confined to friction factor measurements[19–22] which show the axial pressure gradient to be significantly below that in circular ducts when the equivalent diameter is used, as may be expected with such a very non-circular duct. The measurements are conflicting however, ranging from 30 to 60 per cent below the circular duct data, as can be seen from Figure 12. The only local measurements that appear to be

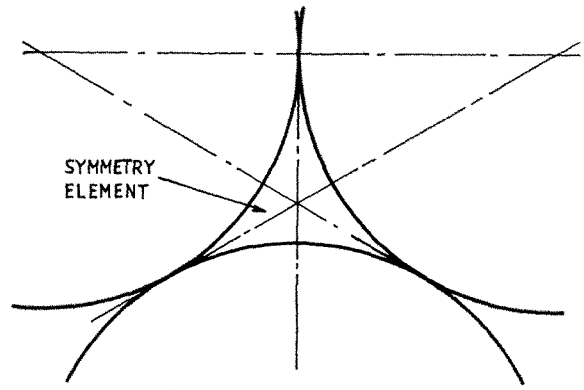

Figure 2. Geometric duct symmetries

available are the axial velocity and wall shear stress distributions reported by Levchenko *et al.*[19] These measurements, which form the main basis of comparison with the present predictions, did not include secondary flow measurement but yielded axial velocity contours which bulge markedly into the duct corners (see Figure 7), thus implying convective transport by secondary flow from the core towards the corners. These effects, including the implied secondary flow circulations, will be discussed in more detail later.

In the present study, a numerical finite volume procedure, developed for the prediction of fully developed turbulent flow in straight passages of arbitrary constant cross-section,[10,23] is applied to a symmetry sextant of the duct, as shown in Figure 2. The method solves the Reynolds, continuity and turbulence transport equations on an orthogonal curvilinear mesh which is generated numerically to fit the duct cross-section.

THE GOVERNING EQUATIONS

The Reynolds equation for steady time-averaged incompressible turbulent flow can be written in Cartesian tensor form as

$$\partial(\rho u_i u_j)/\partial x_i = -\partial p/\partial x_j + \partial(\Gamma_{ij})/\partial x_i \tag{1}$$

and the continuity equation as

$$\partial(\rho u_i)/\partial x_j = 0 \tag{2}$$

The stress tensor Γ_{ij} represents the sum of the viscous and turbulent (Reynolds) stresses, i.e.

$$\Gamma_{ij} = \mu(\partial u_i/\partial x_j + \partial u_j/\partial x_i) - \overline{\rho u_i' u_j'} \tag{3}$$

When cast into general orthogonal co-ordinate form with, for example, the aid of the transformation relations of Pope[24] and specialized to fully developed flow in straight passages, equations (1) and (2) can be written:

Direction 1 (cross-plane)

$$\begin{aligned}\partial(h_2\rho u_1 u_1)/\partial\xi_1 + \partial(h_1\rho u_1 u_2)/\partial\xi_2 = &-h_2\partial p/\partial\xi_1 - \partial(h_2\Gamma_{11})/\partial\xi_1 - \partial(h_1\Gamma_{12})/\partial\xi_2 \\ &- h_1 h_2(\rho u_1 u_2 + \Gamma_{12})/r_1 + h_1 h_2(\rho u_1 u_2 + \Gamma_{22})/r_2\end{aligned} \tag{4}$$

Direction 2 (cross-plane)

$$\partial(h_2\rho u_1 u_2)/\partial\xi_1 + \partial(h_1\rho u_2 u_2)/\partial\xi_2 = -h_1\partial p/\partial\xi_2 - \partial(h_2\Gamma_{12})/\partial\xi_1 - \partial(h_1\Gamma_{22})/\partial\xi_2 + h_1h_2(\rho u_1 u_1 + \Gamma_{11})/r_1 - h_1h_2(\rho u_1 u_2 + \Gamma_{12})/r_2 \quad (5)$$

Direction 3 (cross-plane)

$$\partial(h_2\rho u_1 u_2)\partial\xi_1 + \partial(h_1\rho u_2 u_3)/\partial\xi_2 = -h_1h_2\,\mathrm{d}p/\mathrm{d}\xi_3 - \partial(h_2\Gamma_{13})/\partial\xi_1 - \partial(h_1\Gamma_{23})/\partial\xi_2 \quad (6)$$

Continuity

$$\partial(h_2u_1)/\partial\xi_1 + \partial(h_1u_2)/\partial\xi_2 = 0 \quad (7)$$

Here ξ_3 is the straight axial co-ordinate and ξ_1 and ξ_2 are the cross-plane co-ordinates with metric coefficients h_1 and h_2 and local radii of curvature r_1 and r_2, respectively. The latter are given by

$$\left.\begin{aligned} 1/r_1 &= (1/h_1h_2)\partial h_1/\partial\xi_2 \\ 1/r_2 &= (1/h_1h_2)\partial h_2/\partial\xi_1 \end{aligned}\right\} \quad (8)$$

The cross-plane turbulent stresses $\overline{\rho u_1'^2}$, $\overline{\rho u_2'^2}$ and $\overline{\rho u_1' u_2'}$ contained in Γ_{11} etc. cannot be calculated with an eddy viscosity model since no cross-plane velocities would be generated—this being a consequence of the stresses being directly related to co-planar velocity gradients, as with fully developed laminar flow. This means that a higher order turbulent stress model is needed, which usually entails solving the Reynolds stress transport equations for each stress required. This complex multi-equation method has been tried for square ducts[25,26] with mixed success. An alternative simplified approach was however taken by Launder and Ying[9] who developed approximate algebraic versions of the Reynolds stress transport equations for the calculation of square duct flow. These were later generalized by Gessner and Emery[27] who derived an algebraic equation set for the full Reynolds stress tensor.

The starting point of this algebraic stress transport model (ASTM) was the modelled form of the Reynolds stress transport equations obtained by Hanjalic and Launder.[28] These embodied the usual high Reynolds number assumption of isotropy of the small scale motions responsible for dissipation of the stresses and employed a pressure–strain model based on the assumption of approximately homogeneous turbulence. These equations were then simplified by neglecting transport by diffusion and convection as a first-order approximation based on experimental evidence of the relatively small cross-plane (secondary) velocities that occur and the dominance of vorticity production in the near wall region.[4] This removed the partial derivatives of stress so that the remaining degenerate forms could be manipulated into algebraic relations. This was further facilitated by the consistent assumption that only axial velocity gradients were significant in generation terms and also by the implied local turbulence equilibrium which resulted in emergence of the useful relation $G = \rho\varepsilon$ where G is the generation rate of k, the turbulence kinetic energy, and ε its dissipation rate (see equation (16) with convection and diffusion transport omitted). $\rho\varepsilon$ was substituted for the generation G terms (as in equation (18)) whenever they appeared in the manipulation. The final form of the ASTM equation set for the kinetic stresses can be written in general orthogonal co-ordinate form as

$$\overline{u_3'^2} = C_1k \quad (9)$$

$$\overline{u_2'^2} = C_3k - C_2C_4(k^3/\varepsilon^2)(\partial u_3/h_2\partial\xi_2)^2 \quad (10)$$

$$\overline{u_1'^2} = C_3 k - C_2 C_4 (k^3/\varepsilon^2)(\partial u_3/h_1 \partial \xi_1)^2 \tag{11}$$

$$\overline{u_1' u_2'} = -C_2 C_4 (k^3/\varepsilon^2)(\partial u_3/h_1 \partial \xi_1)(\partial u_3/h_2 \partial \xi_2) \tag{12}$$

$$\overline{u_1' u_2'} = -C_4 (k^2/\varepsilon)\partial u_3/h_1 \partial \xi_1 \tag{13}$$

$$\overline{u_2' u_3'} = -C_4 (k^2/\varepsilon)\partial u_3/h_2 \partial \xi_2 \tag{14}$$

where C_1, C_2, C_3 and C_4 are related coefficients. The overall relation between C_1, C_2 and C_3 can be seen by summing equations (9)–(11) to $2k$ and eliminating the velocity gradients with the relation $G = \rho\varepsilon$.

The axial plane shear stresses $\overline{\rho u_1' u_3'}$ and $\overline{\rho u_2' u_3'}$ are seen from equations (13) and (14) to be represented by a gradient diffusion model with an isotropic turbulent viscosity μ_t given by

$$\mu_t = C_4 \rho k^2/\varepsilon \tag{15}$$

In contrast the cross-plane stresses, which are responsible for secondary flows (their gradients appear as sources in equations (6) and (7)), are seen from equations (10)–(12) to depend on strain rates in planes orthogonal to the cross-plane.

The turbulence quantities k and ε, required in the ASTM, were obtained here from the appropriate form of the well-known k–ε two equation turbulence model[29] which, in the present case yield partial differential transport equations of the following form:

$$\partial(h_2 \rho u_1 k)/\partial \xi_1 + \partial(h_1 \rho u_2 k)/\partial \xi_2 = h_1 h_2 G - h_1 h_2 \rho \varepsilon + \partial(h_2(\mu_t/\sigma_k)\partial k/h_1 \partial \xi_1)/\partial \xi_1 + \partial(h_1(\mu_t/\sigma_k)\partial k/h_2 \partial \xi_2)/\partial \xi_2 \tag{16}$$

$$\partial(h_2 \rho u_1 \varepsilon)/\partial \xi_1 + \partial(h_1 \rho u_2 \varepsilon)/\partial \xi_2 = h_1 h_2 C_{\varepsilon 1} \varepsilon G/k - h_1 h_2 C_{\varepsilon 2} \rho \varepsilon^2/k + \partial(h_2(\mu_t/\sigma_\varepsilon)\partial \varepsilon/h_1 \partial \xi_1)/\partial \xi_1 + \partial(h_1(\mu_t/\sigma_\varepsilon)\partial \varepsilon/h_2 \partial \xi_2)/\partial \xi_2 \tag{17}$$

where σ_k and σ_ε are the turbulent Prandtl numbers for k and ε, respectively, and G is the generation rate of turbulence kinetic energy, calculated from

$$G = -\overline{\rho u_1' u_3'}\partial u_3/h_1 \partial \xi_1 - \overline{\rho u_2' u_3'}\partial u_3/h_2 \partial \xi_2 \tag{18}$$

The boundary conditions applied around the duct periphery involved the use of wall functions to bridge between the interior solution and wall surfaces. The functions used were conventional and based on the well-known 'logarithmic velocity law of the wall' which is written

$$u/u^* = (\ln E y^+)/\kappa \tag{19}$$

where u represents the local resultant velocity and

$$y^+ = \rho u^* y/\mu \tag{20}$$

with y the distance from the wall along the appropriate co-ordinate line. u^* is the local friction velocity taken here as

$$u^* = \tau_s/\rho C_4^{1/4} k^{1/2} \tag{21}$$

with τ_s the local wall shear stress. Experimental measurements have confirmed the applicability of the logarithmic velocity law in near wall regions in a wide range of non-circular passages.[1]

The above relations were used to obtain local wall shear stress for solution of the momentum equations and together with the assumption of local turbulence equilibrium also used to obtain relations for the near-wall generation and dissipation of turbulence kinetic energy for solution of the turbulence equations.[23]

The values of the various constants and coefficients appearing in the foregoing equations, many of which are dependent, were taken as follows from previous work.[7,9,23] $C_2 = 0{\cdot}013$, $C_3 = 0{\cdot}56$, $C_4 = 0{\cdot}085$, $C_{\varepsilon 1} = 1{\cdot}55$, $C_{\varepsilon 2} = 2{\cdot}0$, $\sigma_\varepsilon = 1{\cdot}2$, $\sigma_k = 1{\cdot}0$, $\kappa = 0{\cdot}42$, $E = 9{\cdot}025$.

THE SOLUTION METHOD

The transport equations (4), (5) and (6) for momentum and (16) and (17) for turbulence can all be cast into the following common form:

$$\partial(h_2\rho u_1\phi)/\partial\xi_1 + \partial(h_1\rho u_2\phi)/\partial\xi_2 = \partial(h_2 D_\phi \partial\phi/h_1\partial\xi_1)/\partial\xi_1 + \partial(h_1 D_\phi \partial\phi/h_2\partial\xi_2)/\partial\xi_2 + S_\phi \quad (22)$$

where ϕ represents any of u_1, u_2, u_3, k or ε. Details of the appropriate exchange coefficient D_ϕ and source S_ϕ for each equation can be found in Table 5.3.1 of Reference 23. The turbulent stresses appearing in these source terms were calculated with the ASTM equations (10)–(14).

A conventional finite volume method was used, based on an orthogonal mesh in the passage cross-plane (see Figure 3) and employing a staggered grid arrangement for cross-plane momentum.[30] Integration of each term in equation (22) across the appropriate control volumes led to finite volume equations of the usual form, i.e.

$$(A_P - S_1)\phi_P = A_N\phi_N + A_S\phi_S + A_E\phi_E + A_W\phi_W + S_2 \quad (23)$$

where $A_P = A_N + A_S + A_E + A_W$ and S_1 and S_2 are coefficients of the linearized sources. The A coefficients contain the combined effects of convection and diffusion approximated by a standard hybrid differencing scheme.[31] Full details of the integrations and resulting equations are given in Reference 23.

The solution procedure consisted of a repeated outer sequence in which the cross-plane momentum and continuity equations were dealt with by the 'SIMPLE' method,[31] and an inner iteration sequence in which the finite volume equations were solved with a conventional line-by-line method based on the well known tri-diagonal matrix algorithm.

Owing to the coupling and non-linearity of the equations solved, convergence of the solution was found to be uncertain. These difficulties were also experienced by other workers solving the full 3D momentum equations in other passage geometries,[7,17,18] who were eventually forced to simplify or to prescribe the signs of the sources in the equations containing cross-plane stresses, which were the main source of the instabilities. In the present method however, no simplifications were made or restrictions imposed as convergence of the solution was obtained through careful linearizing of source terms together with extensive under-relaxation, programme control and the

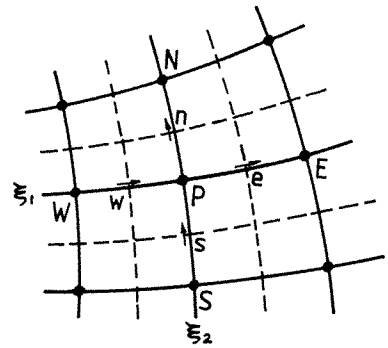

Figure 3. The cross-plane orthogonal curvilinear mesh

use of block adjustment.[23] The convergence requirement used was that the sum of the absolute residual sources over the whole field be less than 10^{-3} of reference quantities based on overall mass and momentum flows.

PREDICTIONS

A finite difference method was used to generate an orthogonal curvilinear mesh fitted into the cross-plane of a symmetry sextant of the duct. In this method, Cartesian co-ordinates x_1 and x_2 are related to the general orthogonal co-ordinates ξ_1 and ξ_2 by the equations[32]

where

$$\left.\begin{aligned} \alpha_2 \partial^2 x_1/\partial\xi_1^2 + \alpha_1 \partial^2 x_1/\partial\xi_2^2 &= 0 \\ \alpha_2 \partial^2 x_2/\partial\xi_1^2 + \alpha_1 \partial^2 x_2/\partial\xi_2^2 &= 0 \\ \alpha_1 = (\partial x_1/\partial\xi_1)^2 + (\partial x_2/\partial\xi_1)^2 &= h_1^2 \\ \alpha_2 = (\partial x_1/\partial\xi_2)^2 + (\partial x_2/\partial\xi_2)^2 &= h_2^2 \end{aligned}\right\} \tag{24}$$

The above were solved by finite differences using central differencing and a similar ADI algorithm to that used in the flow solution. Boundary conditions were calculated by imposing the Cauchy–Riemann conditions mid-way between the boundary and the nearest internal nodes and simultaneously with the boundary shape equations. This is diagrammatically illustrated in Figure 4 with a typical full mesh generated for the present case shown in Figure 5.

Numerical accuracy of the flow solution was tested with laminar flow calculations, grid refinement and comparisons of solutions obtained with different mesh spacings. The laminar flow solutions obtained were found to be within 0·5 per cent of the previously published point matching solutions.[33] In turbulent flow calculations, careful differencing of the source terms on the

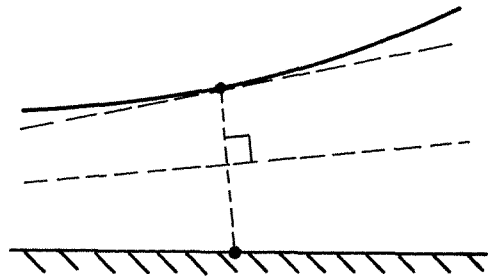

Figure 4. Mesh boundary conditions

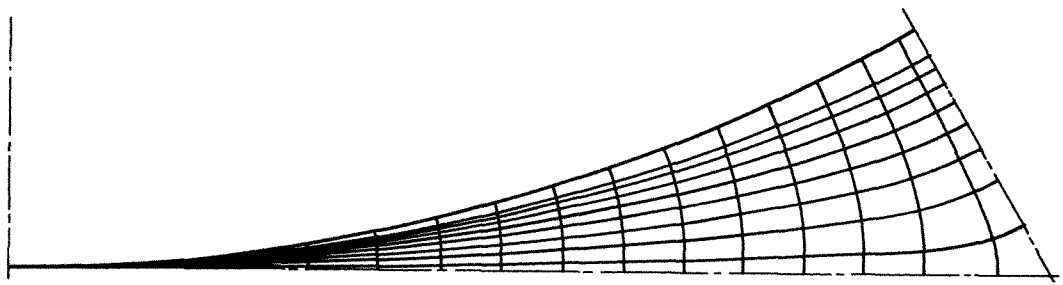

Figure 5. Typical orthogonal mesh

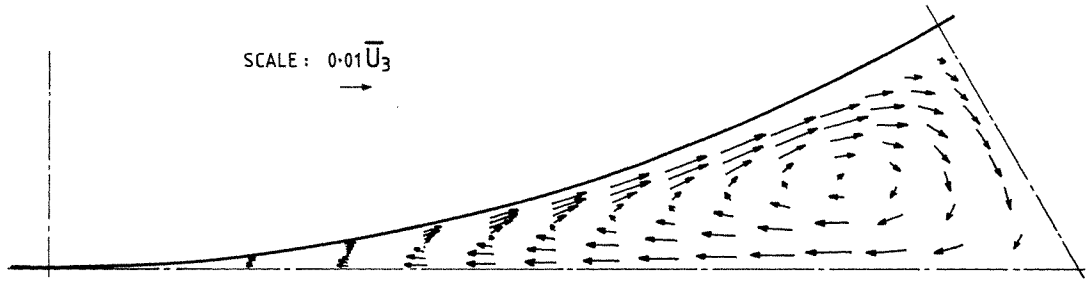

Figure 6. Predicted secondary velocity vectors, $Re = 95{,}000$

orthogonal curvilinear mesh was found necessary, particularly the terms containing cross-plane stresses, to avoid local effects due to mesh geometry. Extensive symmetry tests with different passage geometries were needed to establish differencing methods that eliminated these effects.[23] With the present passage shape, tests with different meshes were used to obtain mean flow solutions that were substantially independent of the mesh. As may be expected, the secondary flow field was found to be more sensitive to mesh changes than mean flow particularly in the regions where nodes became sparse. Of particular interest was the calculated mean flow and turbulence fields in the cusped corner region where the near wall node was close to the viscous sublayer and thus could not be considered in the fully turbulent region as assumed in the modelling of the turbulence equations and in the logarithmic velocity law based wall functions. However, as will be shown, the k–ε model yielded low values of turbulent viscosity in this region and whether the logarithmic law or a simple laminar flow relation was used in the near wall region, negligible changes occurred in the solution. Thus no special modifications of the turbulence model were found necessary to cope with this region. Check calculations were made using a range of meshes in the corner region and only negligible changes occurred in the main flow solution. It appears that this relatively stagnant region has only a minor influence on the main flow. In the solutions presented, the minimum y^+ value at which the logarithmic velocity law was applied was 6·6, this being in the cusped corner region where the flow was close to laminar.

A single circulation of secondary flow was predicted in a symmetry sextant, as seen in the plot of calculated secondary velocity vectors in Figure 6. Flow is from the core into the corner, recirculating to the core via the wall and wall normal with maximum velocities of 1·5 per cent of the mean axial velocity occurring along the corner bisector and near the wall. Although no measurements are available for this geometry, the pattern is similar to that measured by Tahir and Rogers[8] in a triangular array rod bundle with $P/D \equiv 1{\cdot}06$ and is consistent generally with observed

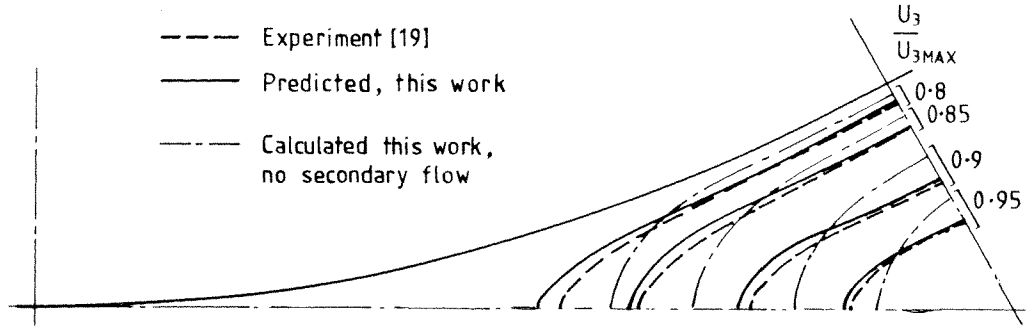

Figure 7. Axial velocity contours, $Re = 42{,}600$

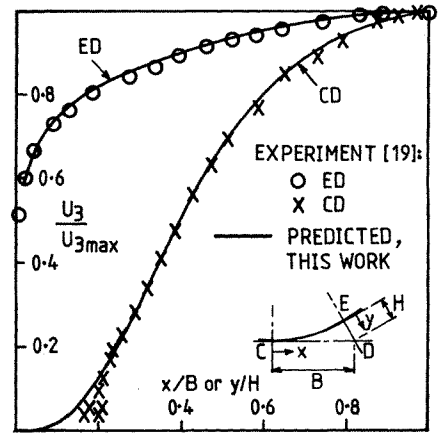

Figure 8. Axial velocity profiles, $Re = 42{,}600$

secondary flow patterns as previously mentioned. The predicted secondary flow pattern of Figure 6 can thus be considered plausible.

The effect of this circulation on the axial velocity contours can be seen in Figure 7 which compares predictions with experiment and with calculations with secondary flow suppressed. The predictions are seen to be in good agreement with experiment and show markedly the characteristic bulging of the contours into the duct corners due to the convective transport of core fluid in that direction by secondary motions. An opposite effect can be seen in the wall region towards $\theta = 30°$ where the contours bend away from the wall due to secondary flow convection transport of near wall fluid away from the wall in that region. Both of these effects appear to be well predicted. θ is defined in Figure 9.

More detail of the axial velocity field is given in Figure 8 which compares profiles plotted along the main symmetry planes and confirms the satisfactory agreement between predictions and measurements. This level of agreement is continued in the wall shear stress profiles displayed in Figure 9. The effect of secondary flow in reducing the peripheral variation is evident with reduced

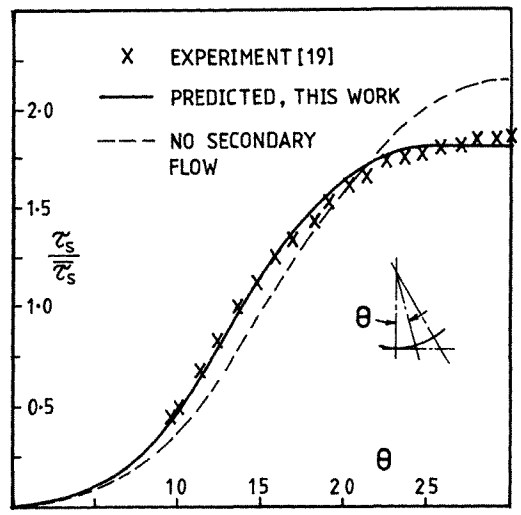

Figure 9. Wall shear stress, $Re = 95{,}000$

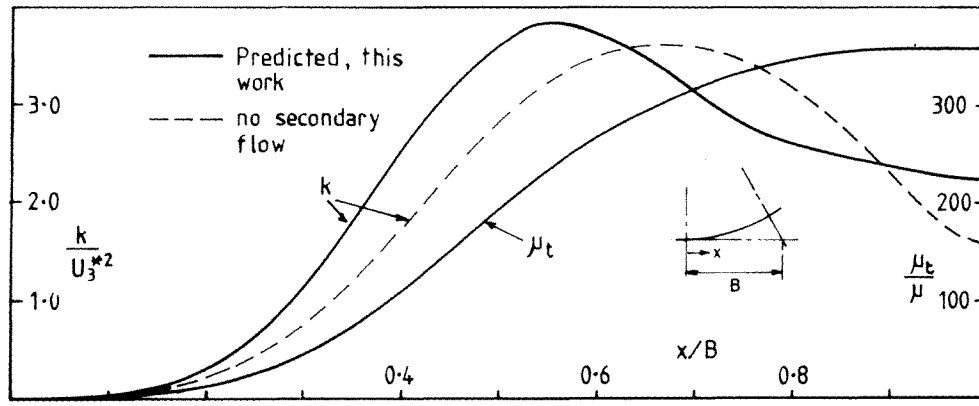

Figure 10. Turbulence profiles along corner bisecting plane, $Re = 95{,}000$

shear stress as θ approaches 30°, owing to the peripheral coupling of the flow field provided by the secondary flow and also the reduced axial velocity gradients in the wall region near $\theta = 30°$ caused by the previously described secondary flow convection transport in that region. This tendency of secondary flow to make wall shear more uniform is apparent in all previous non-circular passages studied [7,9,17,23] and can be considered a further characteristic effect of secondary flow on the mean flow.

Figure 10 gives some details of the turbulence field as predicted by the ASTM and k–ε turbulence models. Unfortunately there are no experimental measurements available for comparison with this geometry. The increased axial velocity gradients into the corner along the corner bisecting plane have increased turbulence kinetic energy generation and have thus shifted the point of maximum k nearer to the corner, as seen in Figure 10. The levels of turbulence kinetic energy and turbulent viscosity are seen to decay rapidly from this point into the corner to give viscosities approaching

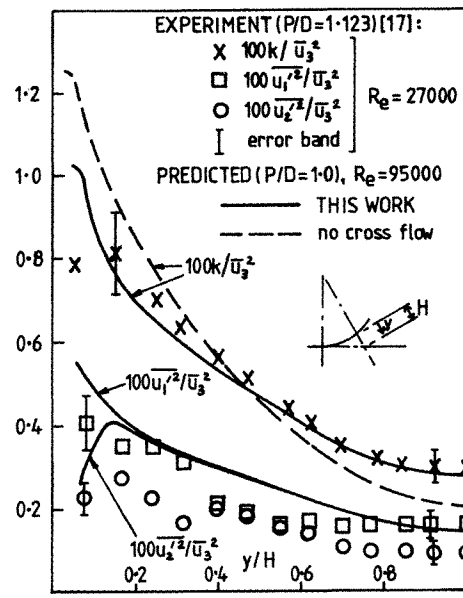

Figure 11. Turbulence profiles along radial symmetry plane

laminar in the last 20 per cent of the centre plane. This is the expected behaviour due to the damping effect of the walls in this cusped corner region and is consistent with the previously mentioned checks made with wall functions at the near wall nodes in this region where replacing the logarithmic velocity law by a simple laminar relation had only a negligible effect on the solution.

The predicted turbulence kinetic energy and cross-plane normal stress profiles along the $\theta = 30°$ symmetry radial plane are shown in Figure 11. In this Figure the laser-Doppler measurements of Carajilescov and Todreas[17] for $P/D = 1{\cdot}123$ are also included to give a comparison with the nearest geometry rod bundle experiments available. The predictions show the same core levels as the measurements and similar general trends in radial variations, particularly for turbulence kinetic energy.

As may be expected from the features of mean flow already discussed in this region, secondary flow has significantly reduced the level of k in the wall region and increased it in the core—as may be observed from the predicted profiles. The comparison between prediction and experiment is not so satisfactory for the cross-plane normal stresses. The measurements show an unexpected anisotropy in the core which was not found by the other experiments at higher P/D ratios.[34,35] This may well be an indication of the uncertainty of such measurements. This anisotropy of the measured stresses near the wall, due to the damping effect of the wall on the normal component $\overline{u_2'^2}$ is a little uneven but apparent and expected. However, the calculated stresses show the damping effect to be confined to the region close to the wall only. This underpredicted wall damping effect obtained when using the ASTM has been discussed before by one of the originators of the model[36] and is a consequence of the model coefficients, particularly C_2, being selected to match homogeneous shear flow rather than near wall equilibrium flows. This method provides satisfactory prediction of secondary flows as evident in the past and present work. Full discussions on stress prediction with the ASTM, mainly in the context of circular and square duct flows, can be found elsewhere.[23,37]

Finally, the predicted friction factor characteristic is compared with the available experiments in Figure 12 where it is seen to be in reasonable agreement with the measurements of Eiffler and Nijsing[22] and Levchenko *et al.*[19] The Sutherland and Kays[21] measurements appear to be significantly lower than these, a result for which there does not appear to be any explanation—particularly since the measured characteristics for other rod bundle P/D ratios presented by them on the same plot are in fair agreement with other published experiments for similar P/D ratios. The

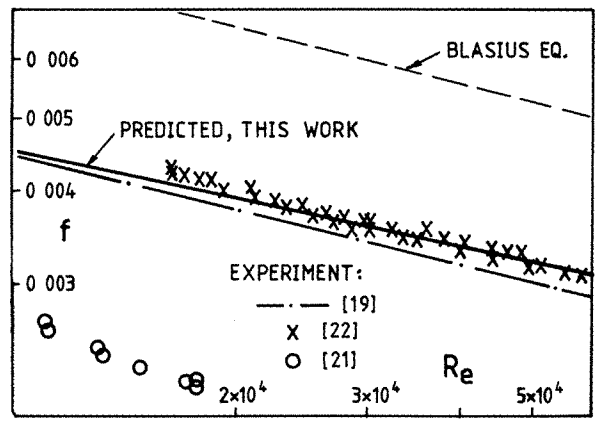

Figure 12. Friction factor characteristics

characteristics in Figure 12 are seen to be all well below the circular duct data, as represented by the Blasius equation, thus indicating that the equivalent diameter concept does not apply, since it would over-estimate pressure drop by more than 70 per cent in this case. This is not surprising since the cusped shape of the duct gives rise to significant variations in wall shear stress, as seen in Figure 8, which makes it far removed from the circular duct case where wall shear stress is uniform. Indeed the very non-circular shape of this duct was the reason for its selection in this study.

CONCLUSIONS

The prediction method developed for fully developed flow in arbitrary shaped passages has been successfully applied to the difficult case of turbulent flow in the cusped cornered duct formed when rods touch in triangular array. A single swirl of secondary flow was predicted in a symmetry one-sixth of the duct and good agreement between predicted and measured local and overall mean flow has been obtained with the convective transport effects of secondary flow clearly evident in the predictions. The k–ε two equation turbulence model, which was coupled with the algebraic stress transport model for stress calculations, appears to have performed adequately. The difficulties expected in the cusped corner region which should contain transition flow did not materialize in the solutions obtained, which yielded plausible turbulence fields. However, since the turbulence model used was valid only for fully turbulent flow it cannot be expected to calculate transition flow properly and the implication is that the relatively stagnant cusped corner region flow does not have a significant influence on flow in the remainder of the duct. It remains to be seen, in the further development of the method for heat transfer prediction, what difficulties may occur due to the viscous effects in this corner region when heat flux is calculated there.

REFERENCES

1. C. W. Rapley, 'A summary of experimental turbulent non-circular passage flow and heat transfer', *Mech. Eng. Report FS*/80/41, Imperial College, London, 1980.
2. C. W. Rapley, 'The simulation of secondary flow effects in turbulent non-circular passage flows', *Int. j. numer. methods fluids*, **2**, 331–347 (1982).
3. J. Nikuradse, 'Turbulent flow in non-circular shaped pipes', (in German), *Ing.-Arch.*, **1**, 306 (1930).
4. E. Brundrett and W. D. Baines, 'The production and diffusion of vorticity in duct flow', *J. Fluid Mech.*, **19**, 375 (1964).
5. B. E. Launder and W. M. Ying, 'Secondary flows in ducts of square cross-section', *J. Fluid Mech.*, **37**, 289 (1972).
6. F. B. Gessner and J. B. Jones, 'On some aspects of fully developed turbulent flow in rectangular channels', *J. Fluid Mech.*, **23**, 689 (1965).
7. A. M. M. Aly, A. C. Trupp and A. D. Gerrard, 'Measurement and prediction of fully developed turbulent flow in an equilateral triangular duct', *J. Fluid Mech.*, **85**, 57 (1978).
8. A. Tahir and J. T. Rogers, 'The mechanism of secondary flows in turbulent interchange in rod bundles', *Proc. 7th Canadian Congress App. Mech.*, 773 (1979).
9. B. E. Launder and W. M. Ying, 'Prediction of flow and heat transfer in ducts of square cross-section', *Proc. I. Mech. E.*, **187**, 455 (1973).
10. A. D. Gosman and C. W. Rapley, 'Fully developed flow in passages of arbitrary cross-section', in C. Taylor and K. Morgan (eds), *Recent Advances in Numerical Methods in Fluids*, Pineridge Press, Swansea, 1980.
11. R. G. Deissler and M. F. Taylor, 'Analysis of axial turbulent flow and heat transfer through banks of rods or tubes', *Proc. Reactor Heat Transfer Conf.*, Paper No. TID7829, New York, 1956.
12. O. E. Dwyer, 'Analytical study of heat transfer to liquid metals flowing in-line through closely packed rod-bundles', *Nuc. Sc. & Eng.*, **25**, 343 (1966).
13. M. H. Ibragimov *et al.*, 'Calculation of the tangential stresses at the wall of a channel and the velocity distribution in the turbulent flow of a fluid', *Soviet Atomic Energy*, **21**, 731 (1966).
14. R. Nijsing, I. Gargantini and W. Eiffler, 'Analysis of fluid flow and heat transfer in a triangular array of parallel heat generating rods', *Nuc. Eng. & Design*, **4**, 375 (1966).
15. R. Nijsing, 'Heat exchange and heat exchangers with liquid metals', *Report AGARD-LS-57-72*, 1972.
16. R. Meyder, 'Turbulent velocity and temperature distributions in the central sub-channel of rod bundles', *Nuc. Eng. & Design*, **35**, 181 (1975).
17. P. Caragilescov and N. E. Todreas, 'Experimental and analytical study of axial turbulent flows in an interior sub-channel of a bare-rod bundle', *J. Heat Transfer, Trans. ASME*, **98**, 262 (1976).

18. A. C. Trupp and A. M. M. Aly, 'Predicted turbulent flows in triangular array rod bundles', *J. Fluid Eng., Trans. ASME*, **101,** 354 (1979).
19. Y. D. Levchenko, V. I. Subbotin and P. A. Ushakov, 'The distribution of coolant velocity and wall stress in closely packed rods', *Soviet Atomic Energy*, **22,** 262 (1968).
20. V. I. Subbotin, P. A. Ushakov and B. N. Gabrianovich, 'Hydraulic resistance to the flow of a liquid along a bundle of rods', *Soviet J. Atomic Energy*, **9,** 848 (1961).
21. W. A. Sutherland and W. M. Kays, 'Heat transfer in parallel rod arrays', *Report GEAP-4637*, 1965.
22. W. Eiffler and R. Nijsing, 'Experimental investigation of velocity distribution and flow resistance in a triangular array of parallel rods', *Nuc. Eng. & Design*, **5,** 22 (1967).
23. C. W. Rapley, 'Fluid and heat flow in tubes of arbitrary cross-section', *Ph.D. Thesis*, University of London, 1980.
24. S. B. Pope, 'The calculation of turbulent recirculating flows in general orthogonal co-ordinates', *J. Comp. Physics*, **26,** 197 (1978).
25. D. Naot, A. Shavit and M. Wolfshtein, 'Numerical calculations of Reynolds stresses in a square duct with secondary flow', *Wärme-und-Stoff.*, **7,** 151 (1974).
26. G. Reece, 'A generalised Reynolds stress model of turbulence', *Ph.D. Thesis*, University of London, 1977.
27. F. B. Gessner and A. F. Emery, 'A Reynolds stress model for turbulent corner flows, Part I', *J. Fluid Eng. Trans., ASME*, **92,** 261 (1976).
28. K. Hanjalic and B. E. Launder, 'A Reynolds stress model of turbulence and its application to asymmetric boundary layers', *J. Fluid Mech.*, **52,** 609 (1972).
29. B. E. Launder and D. B. Spalding, 'The numerical computation of turbulent flows', *Comp. Meth. in App. Mech. and Eng.*, **3,** 269 (1974).
30. F. H. Harlow and J. E. Welsh, 'Numerical calculation of time dependent viscous incompressible flow of fluids with free surface', *Physics of Fluids*, **8,** 2182 (1965).
31. L. S. Caretto *et al.*, 'Two calculation procedures for steady three dimensional flows with recirculation', *Proc. 3rd Int. Conf. Num. Meths Fluid Mech.*, Paris, 60 (1972).
32. A. D. Gosman and R. Johns, 'A simple method for generating curvilinear-orthogonal grids for numerical fluid mechanics calculations', *Mech. Eng. Report FS/79/23*, Imperial College, London (1979).
33. R. A. Axford, 'Multi-region analysis of temperature fields in reactor tube bundles', *Nuc. Eng. & Design*, **6,** 25 (1967).
34. B. Kjellstrom, 'Studies of flow parallel to a rod bundle of triangular array', *Report AE/RV/196*, AB Atomenegi, Sweden, 1971.
35. A. C Trupp and R. S. Azad, 'The structure of turbulent flow in triangular array rod bundles', *Nuc. Eng. & Design*, **32,** 47 (1975).
36. B. E. Launder, written discussion of Reference 27.
37. A. Nakayama, W. L. Chow and D. Sharma, 'Calculation of fully developed turbulent flows in ducts of arbitrary cross-section', *J. Fluid Mech.*, **128,** 199 (1983).